Model Reduction in Discrete-Vortex Methods for Unsteady Airfoil Flows

ArunVishnu SureshBabu *
North Carolina State University, Raleigh, NC 27695-7910

Kiran Ramesh†
University of Glasgow, Glasgow, Scotland G12 8QQ, United Kingdom

and
Ashok Gopalarathnam‡
North Carolina State University, Raleigh, NC 27695-7910

Discrete-vortex methods are a class of low-order methods widely used to study unsteady aerodynamic phenomena. However, these methods demand high computational cost when subject to large number of vortices in the flowfield. This calls for model reduction in discrete-vortex methods. A model reduction technique is applied to a discrete-vortex method called the LESP-modulated Discrete-Vortex Method (LDVM) that was developed in earlier research to study unsteady airfoil flows with leading-edge vortex (LEV) shedding. The criticality of the Leading Edge Suction Parameter (LESP), controls the initiation and termination of LEVs. In this research, model reduction in LDVM is achieved by amalgamating suitable pairs of discrete vortices identified through a condition which requires that the velocity at the airfoil leading edge is not affected by amalgamation. The amalgamated vortex is placed at an optimal location to ensure that the bound circulation and the leading-edge suction are conserved. The reduced-order model is able to predict the flow features and the force and moment coefficients in good agreement with the full model while having significantly lower run times. Use of physical quantities like leading-edge suction and bound circulation enables the easy implementation of this model reduction strategy in other computational methods based on discrete-vortex elements.

Nomenclature

Variables used in the discrete-vortex method

A_0	leading Fourier coefficient

*Graduate Research Assistant, Department of Mechanical and Aerospace Engineering, asuresh2@ncsu.edu.
†Lecturer, School of Engineering, Kiran.Ramesh@glasgow.ac.uk, Member, AIAA.
‡Professor, Department of Mechanical and Aerospace Engineering, agopalar@ncsu.edu, Associate Fellow, AIAA.

A_n	Fourier coefficients
Bxz	body frame
c	airfoil chord, m
C_l, C_d, C_m	airfoil lift, drag, and moment coefficients
C_N, C_S	airfoil normal and suction force coefficients
DV	Discrete Vortex
f	frequency of sinusoidal oscillations of the airfoil, Hz
F_N, F_S	normal and suction forces per unit span of the airfoil, N/m
h	plunge displacement, m
h_{max}	plunge amplitude of sinusoidal oscillations of the airfoil, m
K	non-dimensional pitch rate, $\frac{\dot{\alpha}c}{2U}$
$LESP$	leading-edge suction parameter
M	airfoil moment per unit span, N
OXZ	inertial frame
Re	Reynolds number
r_{core}	core radius of discrete-vortex blobs, m
ρ	freestream density, kg/m^3
T	time period of sinusoidal oscillations of the airfoil, s
t	time, s
t^*	nondimensional time = $\frac{tU}{c}$
U	freestream velocity, m/s
u^k_{ind}, w^k_{ind}	components of velocity induced on k^{th} discrete vortex, m/s
W	downwash on the airfoil, m/s
x, z	chordwise and chord-normal coordinates in body fixed frame, m

x_p	pivot location, from $0-c$, m
x_{ref}	reference point for moment calculation, from $0-c$, m
α	pitch angle, rad
$\dot{\alpha}$	pitch rate, rad/s
Δp	pressure difference across the airfoil, N/m^2
$\delta t, \delta t^*$	dimensional and nondimensional time steps
η	airfoil camber distribution, m
γ	bound circulation distribution, m/s
Γ_b	bound circulation, m^2/s
$\Gamma_{lev,p}$	strength of the latest LEV, m^2/s
$\phi_B, \phi_{lev}, \phi_{tev}$	velocity potential for bound circulation, LEVs, and TEVs, m^2/s
θ	Glauert transformation variable of chordwise distance, rad

Variables used in the amalgamation algorithm

D_0	length parameter, m
d_j, d_k	distance of discrete vortices from leading edge, m
d_{jk}, d_{lk}	distance between discrete-vortex pairs, m
N_{lev}, N_{tev}	total number of LEVs and TEVs
V_0	tolerance on error in induced velocity, m/s
$\bar{X}_j, \bar{X}_k$	position of two discrete vortices considered for amalgamation
(x_{opt}, z_{opt})	optimal location of amalgamated discrete vortices
$\Delta A_0, \Delta A_1$	change in A_0 and A_1 due to amalgamation
$\Gamma_{tev_i}, \Gamma_{lev_j}$	strengths of i^{th} TEV and j^{th} LEV, m^2/s

I. Introduction

Unsteady aerodynamics is a topic of current research interest in a variety of engineering applications such as dynamic stall in wind turbines and helicopter rotors, design of flapping-wing MAVs, wind-energy harvesting, flow control, and gust handling. They are characterized by apparent-mass effects, flow separation, and leading-edge vortex (LEV) formation and shedding [1–4]. Experimental studies that led to the discovery of the critical role of LEVs in insect flight have aided in the development of flapping-wing MAVs [5–8]. The understanding gained from the abundant research on unsteady flappers is currently used in related fields such as in the development of flapping-wing propulsors and aeroelastic wind-energy harvesters[9–12].

Theoretical approaches to study the physics and effects of unsteady aerodynamic phenomena date back to the classical works of Wagner [13] and Theodorsen [14]. The scope of application of many theoretical methods are limited by conventional assumptions like attached flow, small-amplitude motions and planar wakes. Recent interest in high-intensity oscillatory motions of airfoils has shed light on the underlying phenomena in high-intensity unsteady flows that exhibit vortex shedding such as those considered in this paper. Results from parametric studies to characterize the forces and flowfields for such unsteady motions were provided by McGowan et al. [15], Ol et al. [16], Garmann & Visbal [17], and Granlund et al. [18] using both experimental and computational methods. Pitt Ford & Babinsky [19], Baik et al. [20] and Rival et al. [21] have studied the dynamics of leading-edge vortices using experimental techniques while numerical studies on the same have been presented by authors like Visbal and Shang [22] and Ghosh Choudhuri et al. [23].

The cost and time considerations in experimental and computational methods pose a problem in employing them for preliminary design phases where wide range of parameter sweeps might be necessary. This, along with the inherent limitations of purely-theoretical methods, calls for the development of fast low-order models that are based on theory and augmented with the essential physics. Discrete-vortex methods based on potential-flow theory have been popular tools for simulating two dimensional unsteady aerodynamic flows. In these methods, the wake behind the body under consideration and the shear layers representing separated flow are shed from the surface in the form of discrete vortices. A significant advantage of these class of methods over semi-empirical methods is that they are based on the modeled physics and provide a means to study the flow features besides allowing for the calculation of the force coefficients on the airfoil, whereas the latter only allow determination of the force coefficients through empirical fitting [24–26] .

Clements & Maull [27] and Saffman & Baker[28] have reviewed the historical development of discrete-vortex methods. Katz [24] developed a discrete-vortex method for unsteady separated flow past an airfoil to study post-stall aerodynamic behavior of airfoils. Researchers like Sarpkaya [29], Clements [30], Kiya & Arie [31] have applied discrete-vortex methods to other classes of problems like flow past inclined plates and bluff bodies. A review of the applications of vortex methods for flow simulation is given by Leonard [32]. Some of the later efforts to model leading-edge vortices in unsteady flows using discrete vortices for insect flight and MAV-aerodynamics applications

include the low-order methods developed by Ansari et al.[33], Wang & Eldredge[26], Hammer et al.[34], and Ramesh et al. [25] .

Many of the methods mentioned above assume some *ad-hoc* start and stop criteria for vorticity shedding. For example, some methods assume continuous vorticity shedding from the leading edge, which is valid only for a sharp leading edge. A critical value of the local angle of attack controls vorticity shedding in some other methods. This assumption is valid only for a small range of motions. A more general criterion for vortex shedding is required for the application of discrete-vortex methods to a broad class of problems involving different geometries including airfoils with rounded leading edges and arbitrary unsteady motions. Ramesh et al. [25] have developed such a criterion and a discrete-vortex method to model unsteady aerodynamic flows with intermittent LEV shedding. In this method, LEV shedding is modulated using the criticality of a leading-edge suction parameter (*LESP*). When *LESP* is higher than a critical value, discrete vortices are shed from the leading edge of the airfoil so as to maintain the *LESP* at the critical value. This physics-based approach uses only a single empirical constant, the critical *LESP*, which is largely motion independent and needs to be determined only once for a given airfoil and a given Reynolds number. This method (called the *LESP*-modulated Discrete-Vortex Method, or LDVM) is, therefore, ideally suited for modeling oscillatory airfoil flows in which intermittent LEV shedding is a key feature.

While low-order discrete-vortex methods deliver the results in a fraction of the time required by high-fidelity simulations, there is a common limitation. The computational cost of this class of methods is dependent on the number of discrete vortices present in the flowfield. Situations with large number of discrete vortices arise when there is significant vorticity shedding, and in cases where the airfoil undergoes multiple oscillatory cycles. The computational complexity increases as $O(n^2)$, where n is the number of vortices in the flowfield. Fast summation methods are typically used in vortex-particle methods where the number of vortices is in the order of millions. Potential-flow-based prediction methods like those of interest in the current work, where the count is in the order of thousands, calls for an inexpensive approach like physics-based model reduction.

Insights gained from experimental studies about the evolution of the vortex structures help in phenomenological augmentation of low-order models, especially in modeling leading-edge vorticity. The shear layer emanating from the leading edge rolls up into a core, which grows in strength and size as vorticity is fed into this structure by the shear layer. An early attempt in model reduction in discrete-vortex methods is the Brown-Michael model [35] that approximates the vorticity shed from a delta wing by a single concentrated vortex of time-varying strength, thus reducing the complexity to a great extent. The leading-edge vortex pinches off from the shear layer in case of prolonged vorticity shedding and is convected downstream. Meanwhile, a new vortex rollup is initiated near the leading edge [36–38]. A similar approach is used to release matured vortices from the shedding edges in the phenomenological models in [26] and [39]. Antonini et al.[40] use a semi-empirical model for the time-variation of vortex core in a 2D unsteady discrete-vortex method. Sureshbabu et al. [41] present a model-reduction attempt by predicting the phenomena of rollup, growth, and pinch-off

of leading-edge vortices using kinematic conditions.

Inspired by the Brown-Michael model, many researchers have come up with point-vortex models with time-varying vortex strength to represent growing vortex cores. Howe[42] uses the Brown-Michael model with a generalized correction to study the effect of a translating vortex of time-varying strength on a rigid half-plane. Cortelezzi and Leonard [43] model the shear-layer rollup of a semi-infinite plate using a single vortex with time-dependent strength. Wang and Eldredge[26] apply impulse matching for a flat plate to improve on the Brown-Michael model for application in 2D unsteady vortex shedding. Their model has been further revised to obtain a hybrid model that can accommodate a shear layer feeding vorticity into a variable-strength point vortex[39].

A major drawback of representing a concentrated vortex structure by one discrete vortex is that the velocity field inside the structure cannot be accurately replicated without modifying the core radius of the equivalent discrete vortex. The large strength of the discrete vortex will result in substantially high velocities induced in its vicinity. Modeling the variation of core radius of vortices is an area of research that is still being explored. Also, a single discrete vortex cannot represent the flowfield inside a non-circular vortex structure. Due to these problems, the interaction of two large vortical structures cannot be emulated if the structures are replaced by two equivalent discrete vortices. This limitation becomes especially critical in cases where vortex interactions take place close to the airfoil, as noted by [41].

An alternative approach to address the problem of model reduction in discrete-vortex methods is to control the vortex count in the flowfield. A widely used technique for this approach is the amalgamation of discrete vortices [29, 44, 45]. Vortices are amalgamated based on the condition that they are far away from the body and that the flowfield far from the location of the vortices and near the body is not affected significantly [46, 47]. It is important to identify key interactions among vortices to identify vortices for amalgamation. Combining suitable vortices into a single equivalent vortex results in a reduced-order representation of the flowfield. For example, Nair and Taira [48] obtain a sparsified model based on a network-theoretic approach to identify vortex clusters and combine a cluster at its centroid. Xia and Mohseni [49] achieve model reduction by amalgamating discrete-vortex pairs at their centroid. Ramesh et al.[50] controlled the discrete-vortex count in aeroelastic case studies by deleting vortices that crossed a certain distance downstream of the airfoil. Absorption of vortices [47] upon hitting a solid boundary is yet another technique to reduce vortex count, but this approach is not very useful in external flows.

In general, amalgamation, deletion or absorption of discrete vortices require that the vortices be far from the body under consideration if the velocity field near the body is not to be altered. However, it will be advantageous in terms of computational cost to represent the vortical structures near the body with reduced-count discrete vortices, especially for cases that involve intermittent vortex shedding. In this work, a model-reduction strategy is developed for amalgamating discrete vortices including the ones in the vicinity of the body, while preserving bound circulation and flowfield near the leading edge which is an important location on the airfoil with regard to LEV shedding. Discrete-vortex pairs are identified as suitable for amalgamation based on pairwise interactions. Amalgamation of vortices based on such criteria

leads to a natural clustering of vortices so as to exhibit the phenomena like vortex rollup, growth of vortex core through a feeding shear layer, and pinch-off. Representing a vortex core using a finite number of discrete vortices as opposed to using a single point vortex helps to replicate distorted vortex structures like the ones that result from the interaction of two vortex cores. Conventionally, the resulting vortex of an amalgamation process is placed at the centroid. However, this may disturb the flowfield if performed close to the airfoil. The model-reduction strategy presented here finds an optimal location for the amalgamated vortex to minimize the impact of the amalgamation on the flowfield near the airfoil.

The remainder of the paper is organized as follows. The necessary theoretical background for the unsteady aerodynamic model is outlined in Section II. The model reduction strategy applied to the discrete-vortex method is presented in Section III. A comparison of the results and runtime of the reduced-order model with the full model is given in Section IV.

II. Full Aerodynamic Model: Discrete-Vortex Method for Unsteady Airfoil Flows with Leading-Edge Vortex Shedding

The aerodynamic framework used in this study is a potential-flow-based discrete-vortex method developed by Ramesh et al. [25] that is capable of predicting the initiation, shedding, and termination of leading-edge vorticity on airfoils undergoing arbitrary unsteady motions. The backbone of this method is an unsteady thin airfoil theory that can account for large angles and non-planar wakes and that is hence suitable for studying arbitrary unsteady motions with pitch/plunge kinematics. It is built on the time-stepping method outlined by Katz and Plotkin [51]. The essential components of this method are described below. More details can be found in references [25] and [52].

A. Problem setup

The kinematics of the airfoil is depicted in Fig. 1. OXZ represents a stationary inertial frame, while Bxz represents a body-fixed frame attached to the airfoil. The origin B of the body-fixed frame coincides with the leading edge of the airfoil, and the axes x and z are defined to be along the chordwise and the chord-normal directions respectively. At $t = 0$, the body-fixed frame coincides with the inertial frame. For $t > 0$, the airfoil translates to the $-X$ direction (left) with a velocity U, while rotating about the pivot point, x_p, by the pitch angle α. The translational velocity in the Z direction is $\dot{h}$. At any time step, the airfoil is represented by a continuous bound-vortex sheet of strength, $\gamma(\theta, t)$, along its chord given by a Fourier series:

$$\gamma(\theta, t) = 2U \left[A_0(t) \frac{1 + \cos\theta}{\sin\theta} + \sum_{n=1}^{\infty} A_n(t) \sin(n\theta) \right] \tag{1}$$

Here, θ is a variable of transformation relating the airfoil chord, c, to the chordwise coordinate, x, as $x = \frac{c}{2}(1 - \cos\theta)$. Recent research articles have shown that the unsteady Kutta condition requires that the vortex sheet strength is continuous

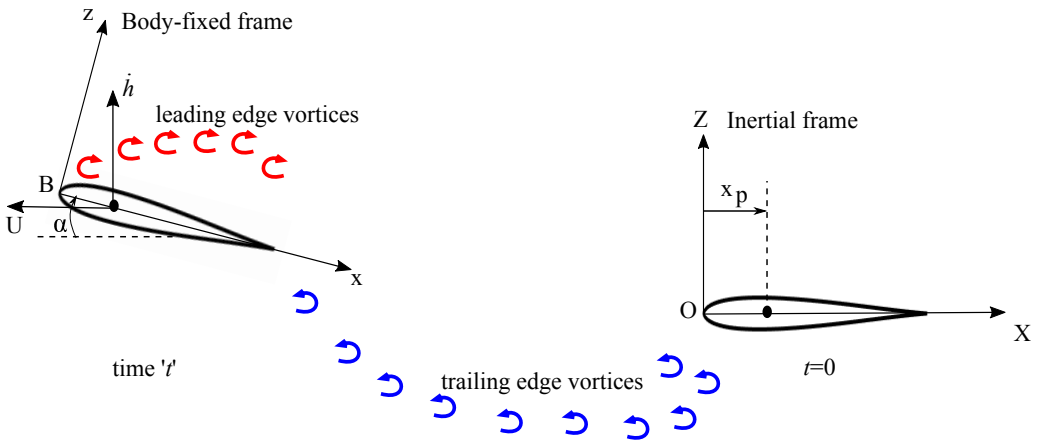

Fig. 1 Illustration of the inertial frame and the body-fixed frame. Airfoil shown at two time instants of 0 and t to illustrate the airfoil kinematics and the schematic representation of discrete-vortex shedding. Translational velocity of the airfoil along X and Z directions are U and $\dot{h}$, respectively.

at the trailing edge [53–55]. However, the current formulation, which is based on the approach of Katz and Plotkin and assumes zero vortex sheet strength at the trailing edge, implicitly enforces the Kutta condition by imposing a zero vortex strength at each time step at the trailing edge which corresponds to $x = c$ and $\theta = \pi$. The time-dependent Fourier coefficients, $A_n(t)$, are calculated from the downwash, $W(x,t)$, which is the normal component of velocity induced on the airfoil surface due to its motion as well as by the discrete vortices in the flow field.

$$A_0(t) = -\frac{1}{\pi}\int_0^\pi \frac{W(x,t)}{U} d\theta \tag{2}$$

$$A_n(t) = \frac{2}{\pi}\int_0^\pi \frac{W(x,t)}{U}\cos n\theta d\theta \tag{3}$$

If ϕ_B, ϕ_{lev}, and ϕ_{tev} are the velocity potentials associated with the bound vorticity, leading-edge vortices and trailing-edge vortices, respectively, the downwash on an airfoil with camberline distribution, $\eta(x)$, can be obtained [25] by imposing the zero-normal-flow boundary condition on the airfoil chord line:

$$W(x,t) \equiv \frac{\partial \phi_B}{\partial z} = \frac{\partial \eta}{\partial x}(U\cos\alpha + \dot{h}\sin\alpha + \frac{\partial \phi_{lev}}{\partial x} + \frac{\partial \phi_{tev}}{\partial x}) - U\sin\alpha - \dot{\alpha}(x - x_p) + \dot{h}\cos\alpha - \frac{\partial \phi_{tev}}{\partial z} - \frac{\partial \phi_{lev}}{\partial z} \tag{4}$$

B. Discrete-vortex shedding

At every time step, a discrete vortex is shed from the trailing edge of the airfoil (referred to as TEVs henceforth). If there is no LEV shedding, the unknown strength of the latest TEV is calculated iteratively so as to satisfy Kelvin's condition.

$$\Gamma_b(t) + \sum_{i=1}^{N_{tev}} \Gamma_{tev_i} + \sum_{j=1}^{N_{lev}} \Gamma_{lev_j} = 0 \tag{5}$$

where Γ_b is the bound circulation of the airfoil.

$$\Gamma_b = \pi c U \left[A_0 + \frac{A_1}{2} \right] \tag{6}$$

LEV shedding is modulated by the Leading-Edge Suction Parameter (*LESP*). Ramesh et al.[25] defined *LESP* as the nondimensional value of the suction peak created at the leading edge:

$$LESP(t) = A_0(t) \tag{7}$$

Ramesh et al.[25] observed that the onset of LEV formation occurs at the same value of *LESP* for a given airfoil at a given Reynolds number, for *any* motion kinematics that results in LEV formation without being preceded by extensive trailing-edge flow separation. Thus, this value, $LESP_{crit}$, represents the maximum suction that an airfoil can support before LEV formation is initiated during an unsteady motion. Once the value of $LESP_{crit}$ is determined for an airfoil at a given *Re* using CFD/experimental data, LDVM can predict the onset and termination of LEV shedding for arbitrary motion kinematics of the same airfoil at that *Re*.

Discrete vortices are shed from the leading edge of the airfoil for those time steps during which *LESP* is above $LESP_{crit}$. The strength of the LEV shed at a time step is determined such that the value of LESP during that time step, which would have been above $LESP_{crit}$, is maintained at the critical value by shedding a discrete LEV. This condition and the Kelvin condition are used to determine the strengths of the TEV and LEV shed when LEV shedding is 'on'. LEV shedding is terminated when *LESP* falls below $LESP_{crit}$.

It is worth mentioning that *LESP* is a generalization of the local flow angle at the leading edge. In steady flow, *LESP* and angle of attack are related by $A_0 = \sin\alpha$. In the current unsteady thin-airfoil theory, the *LESP* value accounts not only for the instantaneous angle of attack, but also for the motion kinematics and the effect of vorticity in the flowfield through the zero-normal-flow boundary conditions in (4).

C. Pressure distribution, forces and moment

The unsteady Bernoulli's equation gives the chordwise distribution of the pressure difference between the lower and upper surface as:

$$\Delta p(x) = p_l(x) - p_u(x) = \frac{\rho}{2}(V_{t_u}^2 - V_{t_l}^2) + \rho \frac{\partial(\phi_u - \phi_l)}{\partial t} \tag{8}$$

As derived in [25], the first term on the right side of (8) can be written as:

$$\frac{\rho}{2}(V_{t_u}^2 - V_{t_l}^2) = \rho \left(U\cos\alpha + \dot{h}\sin\alpha + \frac{\partial \phi_{lev}}{\partial x} + \frac{\partial \phi_{tev}}{\partial x} \right) \gamma(x) \tag{9}$$

In calculating the second term on the right side of (8), the expression for the velocity potentials on either side of the bound-vortex sheet is used:

$$\frac{\partial \phi}{\partial x}(x, 0\pm) = \pm \frac{\gamma(x)}{2} \tag{10}$$

For the time instants when there is no active LEV shedding, the potential difference between the upper and lower surfaces at a location x on the airfoil can be obtained by integration of the bound-vortex sheet strength, using a dummy variable x' to denote the distance along the chord, from the start of the vortex sheet at the airfoil leading edge to x:

$$\phi_u - \phi_l = \int_{x'=0}^{x} \gamma(x')dx' \tag{11}$$

For time instants when there is LEV shedding, because the vortex sheet starts at the edge of the LEV sheet, the potential difference will have an additional term* containing the integral of the leading-edge vortex-sheet strength from the start of the sheet to the airfoil leading edge, as shown in Fig. 2. This additional term, which is equivalent to the sum of the strengths of the discrete LEVs constituting the LEV sheet, results in:

$$\phi_u - \phi_l = \int_{x'=0}^{x} \gamma(x')dx' + \int_{s=0}^{s=s_l} \gamma_{lev}(s) = \int_{x'=0}^{x} \gamma(x')dx' + \sum \Gamma_{lev} \tag{12}$$

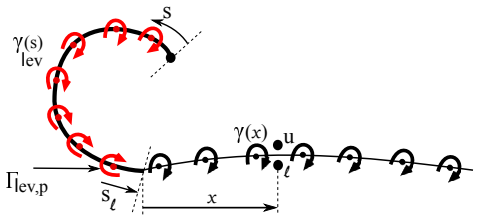

Fig. 2 Schematic for integration of vortex-sheet strength when LEV shedding is active.

The second term on the right side of (8) is then obtained by taking the time derivative of both sides of (12), in which the time derivative of $\sum \Gamma_{lev}$ in the time-stepping approach is simply the strength of the discrete LEV shed in the previous time step, denoted by $\Gamma_{lev,p}$, divided by Δt:

$$\rho \frac{\partial(\phi_u - \phi_l)}{\partial t} = \rho \left(\frac{\partial}{\partial t} \int_{x'=0}^{x} \gamma(x')dx' + \frac{\partial}{\partial t} \sum \Gamma_{lev} \right) = \rho \left(\frac{\partial}{\partial t} \int_{x'=0}^{x} \gamma(x')dx' + \frac{\Gamma_{lev,p}}{\Delta t} \right) \tag{13}$$

*This was pointed out by Prof. Brenden Epps of the Thayer School of Engineering at Dartmouth in a personal communication with the authors.

The normal force per unit span of the airfoil, obtained by integration of $\Delta p(x)$ over the chord, is given by,

$$\begin{aligned} F_N = \rho\pi cU\left[\left(U\cos\alpha+\dot{h}\sin\alpha\right)\left(A_0(t)+\frac{1}{2}A_1(t)\right)+c\left(\frac{3}{4}\dot{A}_0(t)+\frac{1}{4}\dot{A}_1(t)+\frac{1}{8}\dot{A}_2(t)\right)\right] \\ +\rho\int_0^c\left(\left(\frac{\partial\phi_{lev}}{\partial x}\right)+\left(\frac{\partial\phi_{tev}}{\partial x}\right)\right)\gamma(x,t)dx+\rho c\frac{\Gamma_{lev,p}}{\Delta t} \end{aligned} \tag{14}$$

and the suction force per unit span of the airfoil is given by,

$$F_S = \rho\pi cU^2A_0^2 \tag{15}$$

The aerodynamic moment about any reference point x_{ref} on the airfoil is given by:

$$\begin{aligned} M = x_{ref}F_N-\rho\pi c^2U\left[\left(U\cos\alpha+\dot{h}\sin\alpha\right)\left(\frac{1}{4}A_0(t)+\frac{1}{4}A_1(t)-\frac{1}{8}A_2(t)\right)\right. \\ \left.+c\left(\frac{7}{16}\dot{A}_0(t)+\frac{11}{64}\dot{A}_1(t)+\frac{1}{16}\dot{A}_2(t)-\frac{1}{64}\dot{A}_3(t)\right)\right] \\ -\rho\int_0^c\left(\left(\frac{\partial\phi_{lev}}{\partial x}\right)+\left(\frac{\partial\phi_{tev}}{\partial x}\right)\right)\gamma(x,t)xdx-\rho\frac{c^2\Gamma_{lev,p}}{2\Delta t} \end{aligned} \tag{16}$$

The detailed derivation of these expressions are given in Ramesh et al.[25].

The forces can be nondimensionalized using the quantity $\frac{1}{2}\rho U^2c$ to obtain the normal and suction force coefficients C_N and C_S. The coefficients of lift and drag (C_l and C_d) can then be obtained as the force components in the inertial X and Z directions. The moment coefficient (C_m) is obtained as $M/\frac{1}{2}\rho U^2c^2$.

D. Numerical aspects of the discrete-vortex method

The discrete vortices are represented as vortex blobs using the vortex-core model proposed by Vatistas et al. [56], which closely approximates the Lamb-Oseen vortex. The components of velocity induced at a point (x,z) by the j^{th} discrete vortex are given by,

$$u = \frac{\Gamma_j}{2\pi}\frac{z-z_j}{\sqrt{\left[(x-x_j)^2+(z-z_j)^2\right]^2+r_{core}^4}} \tag{17}$$

$$w = \frac{\Gamma_j}{2\pi}\frac{x_j-x}{\sqrt{\left[(x-x_j)^2+(z-z_j)^2\right]^2+r_{core}^4}} \tag{18}$$

A nondimensional time step $\delta t^* = \delta tU/c = 0.015$ is used in LDVM, and the core radius r_{core} of $0.02c$ has been used, which is approximately 1.3 times the average spacing between vortices according to the suggestion by [32]. Each discrete vortex is convected using the total velocity induced at its center by the bound vorticity, the LEVs and the TEVs. For example, the components of velocity induced on the k^{th} LEV at any time step when there are a total of N_{lev} LEVs

and N_{tev} TEVs in the flowfield is given by,

$$u_{ind}^{k} = \sum_{m=1}^{N_{bound}} \frac{\Gamma_m}{2\pi} \frac{(z_k - z_m)}{\sqrt{d_{mk}^4 + r_{core}^4}} + \sum_{j=1}^{N_{tev}} \frac{\Gamma_j}{2\pi} \frac{z_k - z_j}{\sqrt{d_{jk}^4 + r_{core}^4}} + \sum_{l=1}^{N_{tev}} \frac{\Gamma_l}{2\pi} \frac{z_k - z_l}{\sqrt{d_{lk}^4 + r_{core}^4}} \tag{19}$$

$$w_{ind}^{k} = \sum_{m=1}^{N_{bound}} \frac{\Gamma_m}{2\pi} \frac{(x_m - x_k)}{\sqrt{d_{mk}^4 + r_{core}^4}} - \sum_{j=1}^{N_{tev}} \frac{\Gamma_j}{2\pi} \frac{z_k - z_j}{\sqrt{d_{jk}^4 + r_{core}^4}} - \sum_{l=1}^{N_{tev}} \frac{\Gamma_l}{2\pi} \frac{z_k - z_l}{\sqrt{d_{lk}^4 + r_{core}^4}} \tag{20}$$

where $d_{mk} = \left[(x_m - x_k)^2 + (z_m - z_k)^2\right]^{1/2}$, and d_{jk} and d_{lk} are the distances between the corresponding pairs of discrete vortices.

III. Reduced-Order Model

The focus of the current study is to develop a model-reduction strategy for the LDVM framework that can also be easily applied to other discrete-vortex methods. In this paper, a discrete-vortex amalgamation approach is presented to obtain a reduced-order representation of LDVM. Specifically, the challenge is to amalgamate discrete-vortex pairs that are in the vicinity of the airfoil with minimum effect on the flowfield near the airfoil. The vortical structures shed from the edges of the airfoil are represented by a reduced number of discrete vortices, thus retaining the capability of the model to represent distorted structures or interaction of large-scale vortical structures, as explained in Sec. III.B.

A. Identification of vortex pairs for amalgamation

A slightly modified version of Spalart's criterion [47] is used to identify discrete-vortex pairs for amalgamation at every time step. Spalart obtained an expression for the error in velocity at a distant point in the flowfield caused due to the amalgamation of a pair of discrete vortices at their centroid. An amalgamation criterion based on this quantity identifies a pair of discrete vortices to be suitable for amalgamation if the error is smaller than a specified tolerance. The criterion is given by,

$$\frac{\left|\Gamma_j \Gamma_k\right|}{\left|\Gamma_j + \Gamma_k\right|} \frac{\left|\bar{X}_j - \bar{X}_k\right|^2}{(D_0 + d_j)^{3/2}(D_0 + d_k)^{3/2}} < V_0. \tag{21}$$

The left side of (21) represents the error in velocity at a point due to amalgamation of two vortices of strengths Γ_j and Γ_k located at $\bar{X}_j$ and $\bar{X}_k$ into a single vortex of strength $\Gamma_j + \Gamma_k$ located at the centroid of the vortices. The distances of the two vortices from the point are denoted by d_j and d_k . D_0 is a length parameter which is set as 10 percent chord. V_0 has the units of velocity, and is set as the maximum allowed value for the LHS for amalgamation to occur.

In this work, a nondimensional version of Spalart's criterion is used to identify suitable pairs of discrete vortices for amalgamation. The vortex strengths are compared to the quantity cU_∞ and the distances are compared to the chord c. D_0 is retained as $0.1c$. d_j and d_k are taken as the distances of the two vortices from the leading edge of the airfoil. The leading edge of the airfoil is the most sensitive point on the airfoil since the induced velocity at the leading edge is a

major contributor to the suction and hence to the LEV shedding. Hence, it is critical to ensure that the flowfield near the leading edge is not altered due to amalgamation.

The strength factor $\left|\Gamma_j\Gamma_k\right| / \left|\Gamma_j + \Gamma_k\right|$ of the amalgamation criterion primarily encourages amalgamation of vortices with smaller strengths and same signs, and the distance factor $\left|\bar{X}_j - \bar{X}_k\right|^2 / [(D_0 + d_j)^{3/2}(D_0 + d_k)^{3/2}]$ encourages the amalgamation of vortices that are close to each other, and, at the same time, are adequately far away from the airfoil leading edge. Spalart set a tolerance for the left side of (21). However, setting a tolerance to the product of the two factors can lead to selection of vortex pairs for amalgamation because of one of the factors being extremely small even when the other factor is high. For example, a pair of vortices that are far apart might be identified suitable for amalgamation if the corresponding strength factor is small enough so that the product of the factors satisfies the specified tolerance. In the current work, separate tolerances for the strength factor and the distance factor are used to avoid such unrealistic amalgamations.

In the proposed amalgamation strategy, at most one pair of LEVs and one pair of TEVs are identified for amalgamation at every time step. Further, it is ensured that the selected vortices are approaching each other by imposing a requirement that their relative velocity be negative, i.e., toward each other. Among all the pairs that satisfy these tolerance and kinematic requirements, the best pair is chosen as the one with the smallest value for the product of the two factors. The requirements on the strength factor and the distance factor are summarized as:

$$\frac{\left|\Gamma_j\Gamma_k\right|}{\left|\Gamma_j + \Gamma_k\right|} \times \frac{1}{cU_\infty} < 2.5 \times 10^{-3} \tag{22}$$

$$c \times \frac{\left|\bar{X}_j - \bar{X}_k\right|^2}{(D_0 + d_j)^{3/2}(D_0 + d_k)^{3/2}} < 5.0 \times 10^{-3} \tag{23}$$

The tolerance on the distance factor is set such that it permits vortices close to the airfoil to be amalgamated if the pairs are sufficiently close to each other.

B. Placement of the amalgamated vortices

The condition given in (21) is based on the assumption that the amalgamated vortex is placed at the centroid of the pair. Alhough the total momentum of the two vortices is conserved by placing the resultant vortex at the centroid, amalgamation of vortices in the vicinity of the airfoil will inevitably disturb the velocity field surrounding the airfoil. The ensuing error in velocity field will eventually affect the predictions of the model in the future time steps. This will cause the force and flowfield predictions of the reduced-order model to deviate significantly from those of the original model without amalgamation.

Prediction of the flow features at the leading edge like LEV shedding is a key capability of the LDVM method. Therefore, care has to be taken to ensure that the reduced-order model performs well with respect to this capability.

Additionally, the airfoil bound circulation, which is obtained by integrating the circulation distribution, represents the airfoil lift, which is also important to preserve after amalgamation. A heuristic approach is proposed to address these concerns by placing the amalgamated vortex at an 'optimal' location that is, in general, different from the centroid so as to conserve the airfoil bound circulation as well as the leading-edge suction of the airfoil.

In the light of (6) and (7), conserving the bound circulation and the leading-edge suction is equivalent to conserving the two leading Fourier coefficients A_0 and A_1 in the bound-vortex-sheet strength distribution. Thus, in the current amalgamation scheme, each suitable pair of discrete vortices is amalgamated at an optimal location such that A_0 and A_1 are not affected. The strength of the amalgamated vortex is the sum of the strengths of the individual ones.

The errors in A_0 and A_1 due to amalgamation of the vortices at a location (x', z') are given by:

$$\Delta A_0(t) = -\frac{1}{\pi}\int_0^\pi \frac{W(x,t) - W'(x,t)}{U} d\theta \tag{24}$$

$$\Delta A_1(t) = \frac{2}{\pi}\int_0^\pi \frac{W(x,t) - W'(x,t)}{U} \cos\theta d\theta \tag{25}$$

where $W'(x,t)$ is the downwash distribution on the airfoil due to the flowfield with the two discrete vortices replaced by a single vortex at the location (x', z'). The optimal location can then be defined as:

$$(x_{opt}, z_{opt}) = (x', z')|_{\Delta A_0=0,\ \Delta A_1=0} \tag{26}$$

A two-variable Newton-Raphson iterative scheme is employed to determine the location of the amalgamated vortex (x_{opt}, z_{opt}) such that the errors, ΔA_0 and ΔA_1, are less than the tolerance value of 1×10^{-6}. The centroid is used as the starting point for the search. This process typically converges in 5 iterations.

It can be noted that, by considering A_0 and A_1, this amalgamation scheme attempts to take into account the integrated effect of the error in downwash (due to amalgamation) over the entire airfoil, as opposed to the error at a single point. Also, since this approach is based on conserving leading-edge suction and bound circulation, the concept can be extended to other discrete-vortex formulations. The strategy can be translated to other frameworks by obtaining equivalent quantities for leading-edge suction and bound circulation in those frameworks. For example, the equivalent quantity for leading-edge suction has been obtained by Aggarwal [57] for a lumped-vortex-element formulation, and by Darakananda and Eldredge [39] for a conformal-mapping-based model.

IV. Results

The full model, LDVM, was validated against experiment and computation by Ramesh et al. [25] for various motion kinematics and different Reynolds numbers. The LDVM was found to be effective in predicting the intermittent LEV shedding and the resulting fluid-dynamic loads in complex, unsteady airfoil flows. The performance of the

current reduced-order model is compared with that of the full model for three case studies in this section. Force- and moment-coefficient predictions of the reduced-order model are compared with those of LDVM. Also, the flowfield predictions of the two models are compared against each other using streamline plots and discrete-vortex distributions in the region around the airfoil. Comparison with experimental and/or CFD results are also included for completeness. The runtimes of the two models averaged over several executions are reported to show the effect of model reduction. The cases are chosen to present the capability of the reduced-order model to reproduce different flow features observed in the low-Reynolds-number flow regime dominated by LEV shedding. The $LESP_{crit}$ values for all the cases considered in this section were determined by Ramesh et al. [25].

A. Case 1: Pitch-up-hold motion of a flat plate

A pitch-up-hold motion of a flat plate at Re=1,000 is considered in this subsection. The plate is pitched up about its leading edge at a nondimensional pitch rate of $K = \dot{\alpha}c/2U = 0.4$ to an angle of 45 degrees. It is held at that position until the end of the motion at a nondimensional time of $t^* = 9.0$. This type of motion kinematics has been of recent interest to the AIAA Fluid Dynamics Technical Committee Low Reynolds Number Discussion Group. The LDVM was validated by Ramesh et al. [25] for this case against CFD results from a viscous vortex particle method by Eldredge [58]. These CFD results are also included in the current discussion for completeness.

The variations with t^* of the pitch angle, α, and various aerodynamic coefficients are shown in Fig. 3. The flowfields predicted by the full model and the reduced-order model are compared against each other and against the CFD-predicted flowfields in Fig. 4 for four time instants. The discrete-vortex distributions representing the vortex structures and the wake are also co-plotted on the corresponding streamline plots.

Figure 3(a) shows the variations of $LESP = A_0$ from the full and the reduced-order discrete-vortex methods. The $LESP_{crit}$ value for a flat-plate geometry at Re=1,000 was determined in [25] to be 0.11, and is shown in Fig. 3(a). The *LESP* history predicted by the reduced-order model is seen to be in excellent agreement with that of the full model. It is seen that the *LESP* reaches the critical value of 0.11 soon after the plate starts pitching up. It stays at $LESP_{crit}$ until the motion ends, indicating continuous LEV shedding from the upper surface of the flat plate. As a consequence, clockwise discrete vortices are shed at every time step from early in the upstroke to the end of the motion, as seen from the flowfield images in Fig. 4. As seen from the flow images in Fig. 4, the LEV builds up in strength until approximately $t^* = 4$. At this time, the LEV is of a size large enough to induce the trailing-edge shed vortices to roll up into a concentrated TEV over the aft portion of the upper surface of the airfoil. When the TEV grows sufficiently large, it causes a detachment of the LEV from the feeding sheet emanating from the leading edge. The flow physics of the LEV detachment has been explained by [38], in which the authors show that LEV detachment is initiated when the rear stagnation point aft of the LEV on the upper surface of the airfoil (half saddle point), reaches the trailing edge. This process alternates, resulting in a von Kármán vortex street. The flow-visualization snapshots from the reduced-order model are seen to be in excellent

agreement with those from the full LDVM. Vorticity plots from CFD are shown in Fig. 4 for qualitative comparison with the flowfields predicted by the discrete-vortex models. The results of the vortex models are seen to compare well with the vorticity plots from CFD, with minor discrepancies seen in the timing of the pinch-off of the LEV at $t^* = 4$ and the locations and sizes of the vortex structures in the subsequent time instants. The discrepancies between LDVM and CFD results can be attributed to the fact that the viscous effects like formation of thick boundary layers on the airfoil are not modeled in the LDVM theory. Interested readers can refer to [25] for a more detailed discussion of discrepancies between LDVM and CFD.

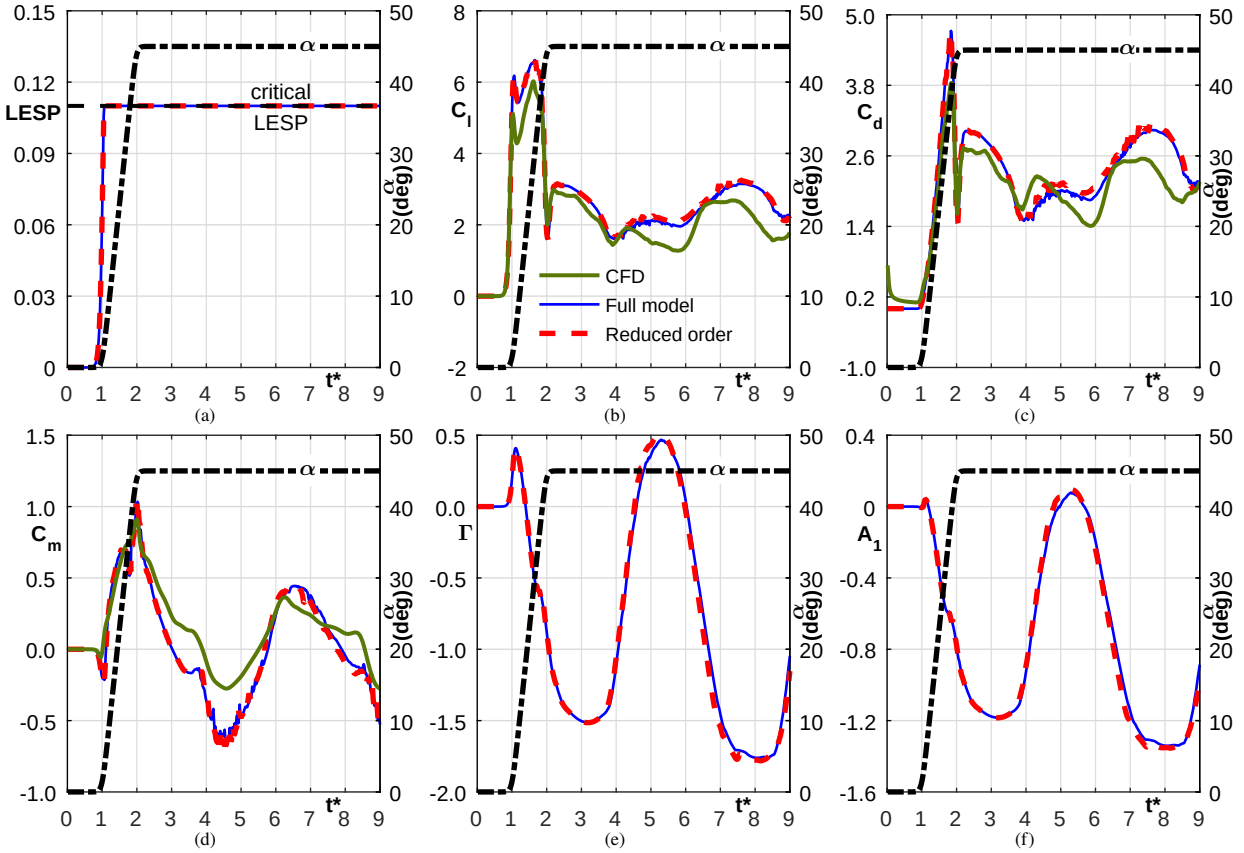

Fig. 3 Case 1: Comparison of predictions of the reduced-order model, the full model, and CFD results of Eldredge [58]. Variations with $t^* = tU/c$ of: (a) *LESP*, (b) lift coefficient, (c) drag coefficient (d) pitching-moment coefficient about the mid chord, (e) bound circulation, and (f) Fourier coefficient A_1.

The lift, drag and moment coefficients predicted by the full model, the reduced-order model, and CFD are co-plotted in the subfigures (b)–(d) of Fig. 3. Comparison between the predictions from the full and the reduced-order models is seen to be excellent for the entire motion. As seen in Figs. 3(e) and (f), the variations of the bound circulation, Γ, and the Fourier coefficient, A_1, predicted by the full and the reduced-order models are seen to be in excellent agreement with each other. It is seen that the reduced-order model exhibits some high-frequency noise in the force results, which is attributed to the rather small, but nevertheless abrupt, force changes between successive time steps due to amalgamation of the vortices. The lift and drag results from the two discrete-vortex methods are seen to agree well with the CFD results

until approximately $t^* = 4$, when the pinch-off of the first LEV occurs followed by alternate LEV/TEV shedding. After this time, although the results from the two methods have some discrepancies, their time histories have similar behavior.

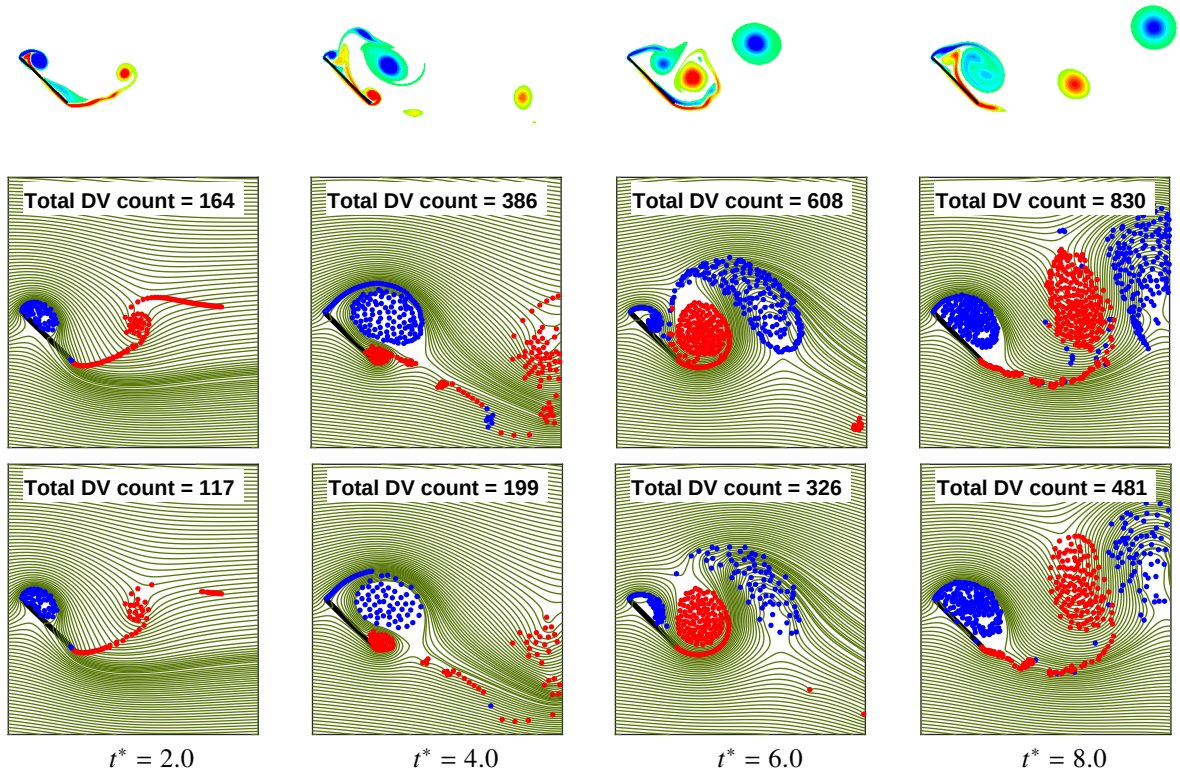

Fig. 4 Case 1: Comparison of flowfield results from CFD (top) of Eldredge [58], full model (middle), and the reduced-order model (bottom) at four time instants. In the discrete-vortex images, clockwise vortices are shown in blue and counterclockwise in red.

Overall, the predictions from the reduced-order model for both the forces and the flowfields are seen to be in excellent agreement with those from the full LDVM. As seen from Fig. 4, this prediction is achieved with a significantly smaller number of discrete vortices in the reduced-order model. The motion sequence comprises of 500 discrete time steps, at the end of which the full model has 940 discrete vortices in the flowfield, while the reduced-order model has only 561 discrete vortices. The smaller discrete-vortex count, achieved through model reduction, results in a reduction in runtime from 25.8 seconds to 13.4 seconds.

Effect of the length parameter D_0 on the performance of the reduced-order model

The parameter D_0 controls the number of amalgamations occurring near the airfoil surface relative to that occuring in the wake. For large values of D_0, the term $(D_0 + d_j)$ encourages amalgamations very close to the airfoil surface, i.e., for even small values of d_j. Thus, larger values of D_0 encourage more amalgamations, and also result in uniform vortex density in the entire flowfield since $(D_0 + d_j)$ does not vary much for small d_j. For smaller values of D_0, $(D_0 + d_j)$ is small near the airfoil, and hence amalgamations very close to the airfoil are discouraged. The effect of varying D_0

on the performance of the reduced-order model for case 1 is demonstrated in Fig. 5. When $D_0 = 1.0c$, the reduction in discrete vortex count is enhanced, with more amalgamations taking place near the airfoil. The computational time saving achieved, however, comes at a cost in accuracy of the force and flowfield predictions, as can be seen from Fig. 5. The results do not seem to vary significantly for smaller values of D_0, in agreement with the observation of Spalart reported in [47]. Spalart suggests a typical value of $0.1c$ for D_0. Hence, this value is chosen for the reduced-order model presented here.

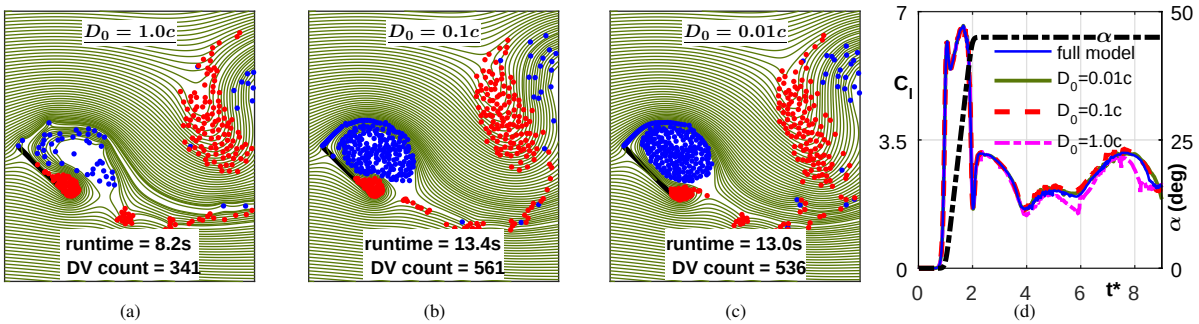

(a) (b) (c) (d)

Fig. 5 Effect of D_0 on the predictions of the reduced-order model for case 1. The flowfield predictions for three values of D_0 are shown in subfigures (a), (b), and (c). The corresponding C_l predictions are co-plotted in subfigure (d).

B. Case 2: Pitch-up-hold-return motion of SD7003 airfoil

In this subsection, the pitch-up-hold-return motion of the cambered SD7003 airfoil at Re = 30,000 is studied. The airfoil is pitched up about its leading edge to a pitch angle of 25 degrees at a nondimensional pitch rate of $K = 0.11$, held at this angle for a short duration, and is then pitched down at the same rate to the initial value of 0 degrees. This motion kinematics is generated using Eldredge function [59]. In earlier work [25], the LDVM predictions for this motion were validated against experimental and CFD results. The experimental lift and drag coefficient data and dye-flow visualization images were obtained from tests performed at the US Air Force Research Laboratory (AFRL) Horizontal Free-surface Water Tunnel. The CFD results for the force and moment coefficients as well as the flowfield were generated using NCSU's REACTMB-INS unsteady RANS code. In earlier work ([25],[60]), the results from the RANS CFD analysis using the Spalart-Allmaras turbulence model, as implemented in REACTMB-INS flow solver, have been shown to agree reasonably well with experimental results for LEV initiation and formation on airfoils operating at Reynolds numbers between 10,000 and 40,000. More details about the experimental and CFD results for this case can be found in [25]. In the current work, results from the reduced-order model are compared against the full LDVM and experimental and CFD results.

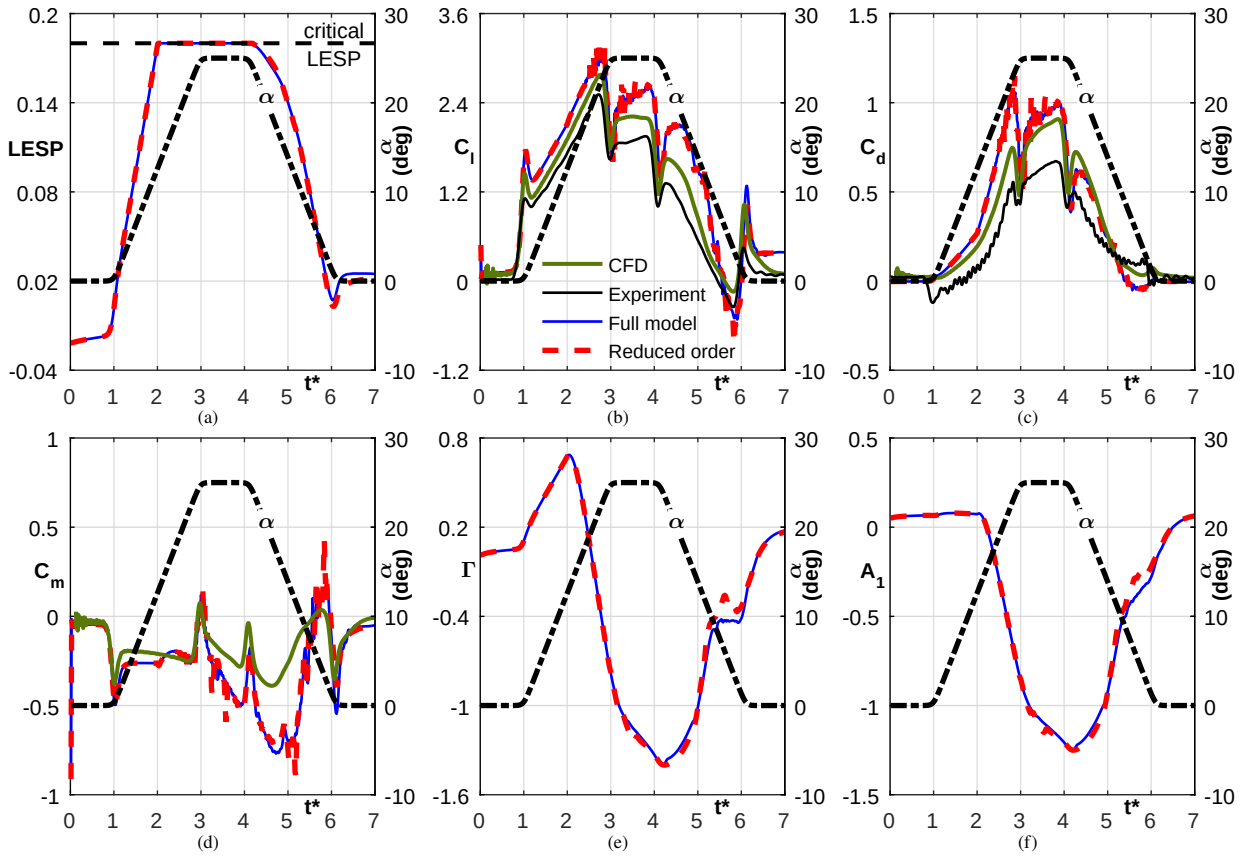

Fig. 6 Case 2: Comparison of predictions of the reduced-order model, the full model, CFD, and experiment. Variations with $t^* = tU/c$ of: (a) *LESP*, (b) lift coefficient, (c) drag coefficient (d) pitching-moment coefficient about the quarter-chord, (e) bound circulation, and (f) Fourier coefficient A_1. Experimental and CFD results are from [25].

The kinematics and time variations of various aerodynamic coefficients are shown in Fig. 6, in which the predictions from the reduced-order model are compared with those from the full LDVM as well as experimental and CFD results. The flowfields predicted by the full and the reduced-order models are compared against each other and qualitatively against the CFD-predicted vorticity-distributions and experimental dye-flow visualizations in Fig. 7 for four time instants. It must be noted that the dye-flow visualization tracks the evolution of a passive scalar (dye concentration) and not the vorticity field. For this reason, the comparison of the dye visualization with the CFD vorticity plots and discrete-vortex flowfields is at best qualitative. In the present situation, it can be argued that the qualitative comparison is appropriate because, first, the diffusion of the dye can be assumed to be small in the present case since the flow visualization is for the initial stage of the vortical flow development over the chord (rather than in the wake), and second, the advection term is the dominant term in the transport equations for the nominally two-dimensional flow in this case [61]. As was done for the earlier case study, the discrete-vortex distributions representing the vortex structures and the wake are also co-plotted on the corresponding streamline plots.

Figure 6(a) shows the variations of $LESP = A_0$ from the full and the reduced-order discrete-vortex models. The

$LESP_{crit}$ value of 0.18 for the SD7003 airfoil at this Reynolds number, taken from the earlier study [25], is also shown in the figure. As seen in the earlier case, the *LESP* history predicted by the reduced-order model is seen to be in excellent agreement with that of the full model. The small deviation in the *LESP* value from that predicted by the full model in the terminal phase of the motion, as well as the spikes in the moment curve can be attributed to amalgamations taking place too close to the airfoil surface. For the motion kinematics used in this case study, the *LESP* increases as the airfoil is pitched up. It reaches the critical value of 0.18 at $t^* = 2$, remains constant before it starts decreasing soon after the airfoil starts pitching down at $t^* = 4$. During the time when the *LESP* is held at the critical value, clockwise LEVs are shed from the leading edge, as seen in the flow images for the full and the reduced-order discrete-vortex models in Fig. 7 for $t^* = 3$ and 4. For these time instants, the LEV structure and position from the two discrete-vortex methods agree well with the flow images from CFD and experiment. When the *LESP* falls below the critical value, LEV shedding in the two discrete-vortex methods stops, and the already-shed LEV convects down the chord, interacting with the vortices shed from the trailing edge at $t^* = 6$. The flow images from the discrete-vortex methods for $t^* = 5$ are in general agreement with that from experiment. The lack of clarity in the dye-flow image for $t^* = 6$ makes it difficult to assess the comparison with experiment for that time instant. On the other hand, there is some discrepancy between the discrete-vortex and CFD flow images for $t^* = 5$ and 6. The CFD shows a second, but smaller, LEV being shed at $t^* = 5$, which is not seen in the discrete-vortex methods. For all time instants, however, it is seen that the flowfield images from the reduced-order model agree well with those from the full LDVM.

The lift and drag coefficients from the full model, the reduced-order model, CFD, and experiment are co-plotted in the subfigures (b) and (c) of Fig. 6. Comparison between the predictions from the full and the reduced-order models is seen to be excellent for the entire motion. As with case 1, it is seen that the reduced-order model exhibits some high-frequency noise in the force results. Comparing the results from CFD and experiment, it can be observed that that C_l from experiment is lower than that from CFD during the hold and downstroke, i.e., from t^* of 3 to 6; C_d from experiment is lower than that from CFD for most of the motion. Second, the two discrete-vortex methods correctly capture the locations and the intensities of the spikes in the C_l and C_d time histories. These spikes are due to apparent-mass effects. From the start of the motion until the end of the hold, i.e., from $t^* = 0$ to 4, C_l from the discrete-vortex methods match reasonably well with CFD predictions. During the downstroke, the discrete-vortex methods over-predict C_l compared to CFD by approximately the same amount by which experiment under-predicts CFD. From subfigure (d) of Fig. 6, it is seen that C_m from the discrete-vortex methods compare excellently with each other and reasonably well with CFD except in the downstroke region, where C_m predictions from the full LDVM and the reduced-order model are noticeably more negative than the CFD prediction. Some of this discrepancy in C_m prediction is again attributed to the formation of thick boundary layers on the upper surface, which is not modeled in the discrete-vortex methods. Pitching moment measurements are not available from experiment. It can be seen from Figs. 6(e) and (f) that the bound circulation and the Fourier coefficient (A_1) histories from the reduced-order model match well with the full-model predictions.

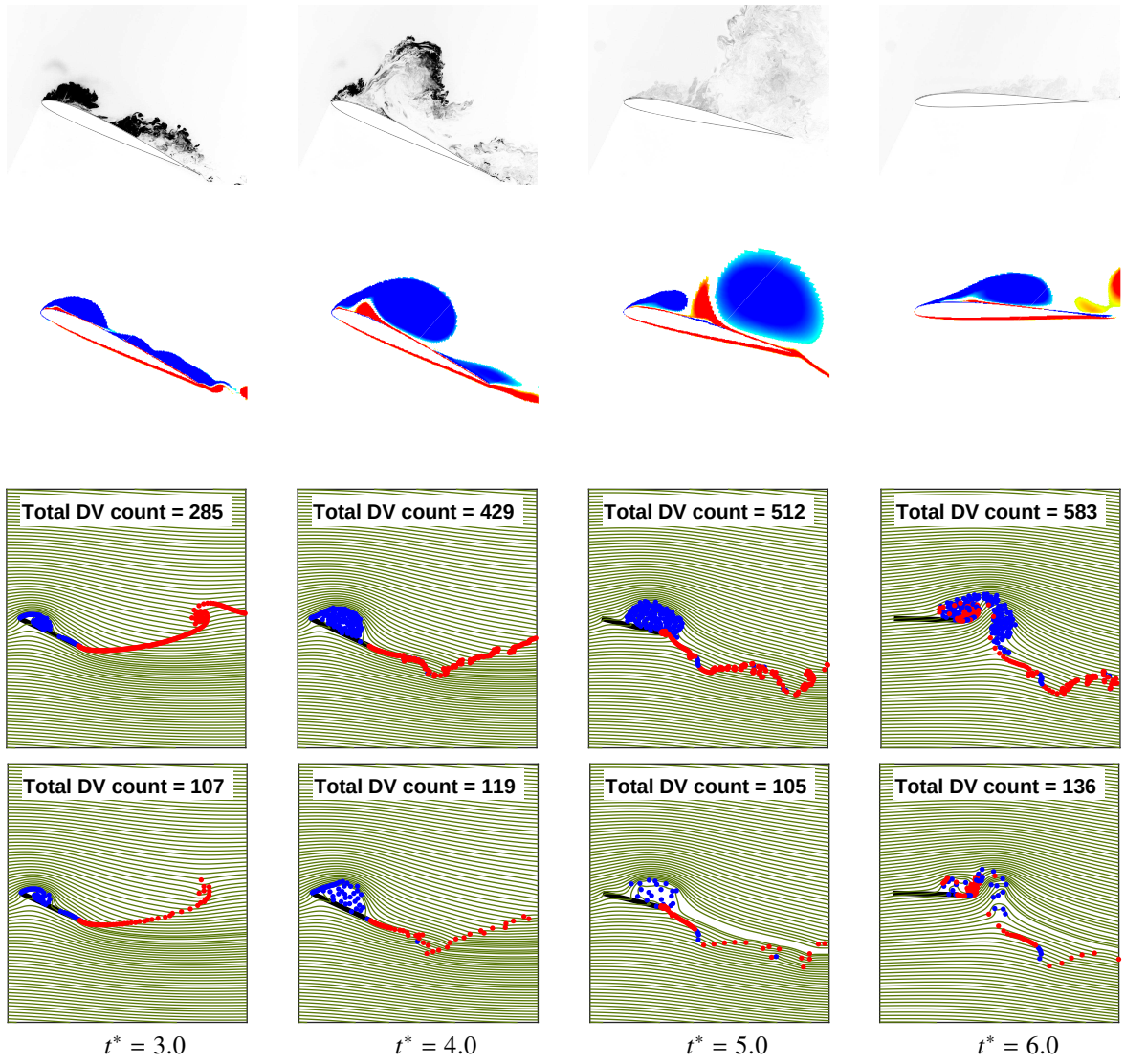

Fig. 7 Case 2: Comparison of flowfield results from experiment (first row), CFD (second row), full model (third row), and the reduced-order model (fourth row) at four time instants. Experimental and CFD images are from [25]. In the discrete-vortex images, clockwise vortices are shown in blue and counterclockwise in red.

As with case 1, the predictions from the reduced-order model for both the forces and the flowfields are seen to be in excellent agreement with those from the full LDVM. This case study shows that the reduced-order model can predict the initiation and termination of LEV shedding in a complex unsteady flow with the same accuracy as the full LDVM. It also showcases the ability of the reduced-order model to replicate the effect of a vortical structure very close to the airfoil surface using a reduced number of discrete vortices without affecting the force/moment predictions, and also to reproduce the interaction of vortical structures without deviations in the flowfield predictions. The number of discrete vortices in a 500-time-step simulation reduces from 655 to 149 as a result of model reduction, causing a significant runtime reduction from 12.6 seconds to 2.7 seconds.

C. Case 3: Sinusoidal pitch-plunge oscillations of a NACA0015 airfoil

In this case study, the sinusoidal pitch-plunge oscillations of a NACA0015 airfoil at a Reynolds number of 1,100 [62] is considered. The airfoil oscillates with a frequency, $f = \omega c/(2U)$, of 0.14 about the pivot point located at one third of its chord. The pitch motion has an amplitude of 76.3 degrees with zero mean. This pitch motion is combined with a sinusoidal plunge oscillation of the same frequency and an amplitude of $h_{max}/c = 1$. Plunge leads pitch by a phase difference of 90 degrees, so that when the pitch angle is zero and decreasing, the plunge displacement is at maximum bottom displacement . This motion was among the several sinusoidal motions analyzed using CFD by Kinsey and Dumas [62] for studying power extraction from oscillating airfoils. LDVM was validated using their results in earlier work [25], in which the $LESP_{crit}$ for a NACA0015 airfoil at a Reynolds number of 1,100 was determined to be ±0.19.

An oscillatory motion, such as the one considered here, leads to periodic LEV shedding from both the surfaces of the airfoil, and a discrete-vortex simulation typically has to be carried out for multiple cycles for cycle-to-cycle convergence to be achieved. For these reasons, such simulations result in a large number of discrete vortices in the flowfield of the full model, and thus require longer computation times. Hence, this case is a good candidate for studying the ability of the reduced-order model to modulate alternate LEV shedding from the two surfaces of the airfoil, and for highlighting the effectiveness of model reduction in scenarios with large discrete-vortex count.

For this case study, three cycles of oscillations are studied using 1,500 discrete time steps for both the full and the reduced-order discrete-vortex methods. The kinematics and time variations of various aerodynamic coefficients are shown in Fig. 8 for the third cycle, in which the predictions from the reduced-order model are compared with those from the full LDVM as well as the CFD results from [62]. The results are plotted against a non-dimensional time, t/T, where T is the time period of the sinusoidal oscillations. The flowfields predicted by the full and reduced-order models are compared against each other in Fig. 9 for four time instants in the third cycle of the motion. As was done for the earlier cases, the discrete-vortex distributions representing the vortex structures and the wake are also co-plotted on the corresponding streamline plots.

Figure 8(a) shows the variations of $LESP = A_0$ from the full and the reduced-order discrete-vortex methods. As in earlier cases, the *LESP* variation predicted by the reduced-order model is seen to compare excellently with that from the full LDVM. It is seen that, at $t/T = 0$, the *LESP* decreases, then reaches and stays constrained at the negative critical value of *LESP* from t/T of approximately 0.1 to 0.4. During this time, counterclockwise vortices are shed from the leading edge in the discrete-vortex methods, which convect to the lower surface of the airfoil, as seen from the flow images for $t/T = 0.25$ in Fig. 9. Between t/T of approximately 0.4 and 0.65, the *LESP* increases from the lower critical value to the upper critical value. During this time, as seen from the flow visualization for t/T of 0.5 and 0.75 in Fig. 9, LEV shedding briefly stops before resuming with shedding of clockwise discrete vortices which convect over the upper surface of the airfoil. At approximately t/T of 0.9, the *LESP* falls below the positive critical value and start decreasing, resulting in another pause in the LEV shedding, as seen from the flow visualization for t/T of 1.0 in Fig. 9. Thus, in

every cycle of the sinusoidal motion, the *LESP* variation gets alternately constrained at the negative and positive critical values and results in alternate shedding of counterclockwise and clockwise vortices, which then convect along the lower and upper surfaces of the airfoil, respectively. It is seen from the flow-visualization results in Fig. 9 that the flow predictions from the reduced-order model compare excellently with those from the full LDVM even for the intermittent and alternate LEV shedding seen in this case study. Figures 8(b)–(d) compare the variations of C_l, C_d, and C_m from the reduced-order model with those from the full LESP and CFD. Figures 8(e)–(f) compare the variations of Γ and A_1 from the two discrete-vortex methods with each other. In all these plots, it is seen that the results of the reduced-order method compare excellently with those of the full LDVM. When comparing the results from the two discrete-vortex methods with those from CFD, it is seen that the comparison in lift is seen to be very good and the comparison in drag is excellent. As with the other cases, pitching-moment prediction from the discrete-vortex methods is seen to have some discrepancies compared to the CFD result, but the general behaviour is similar to that seen in the CFD results.

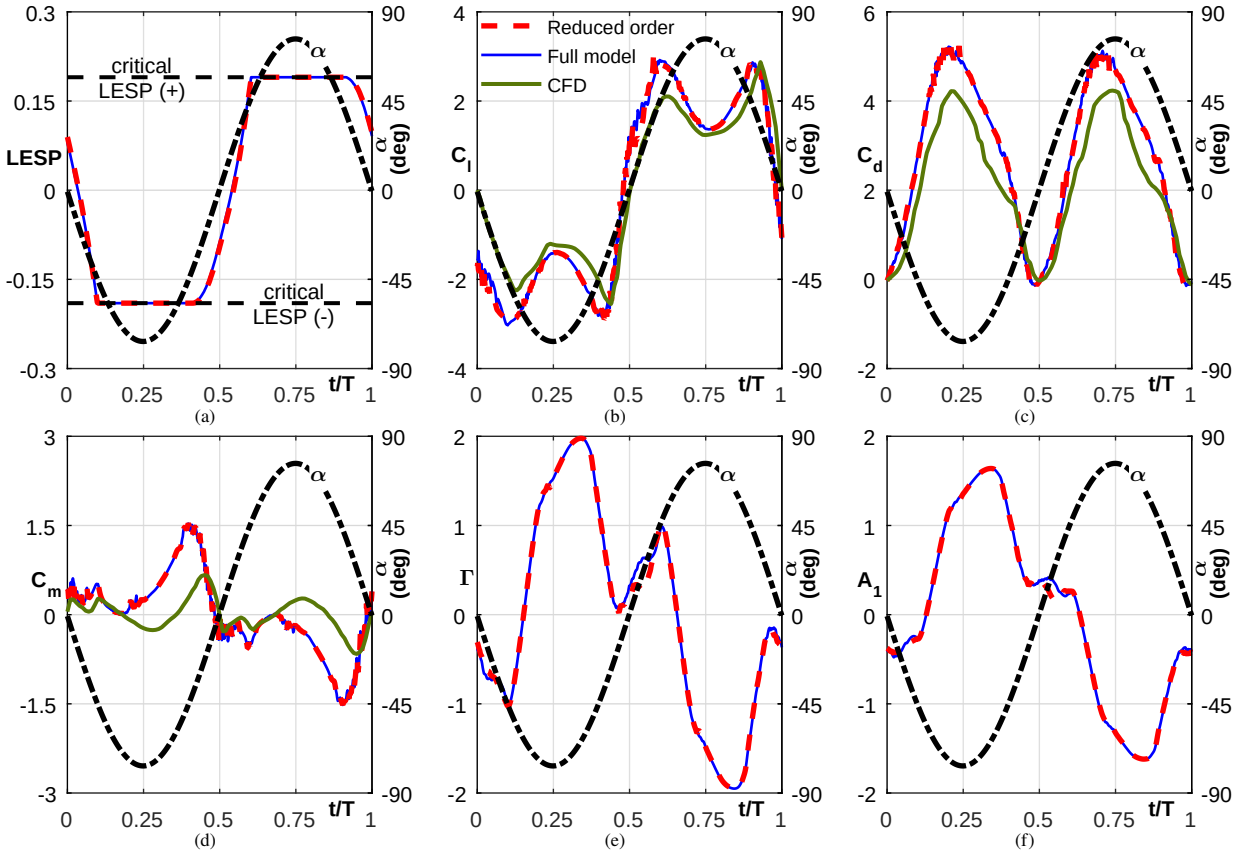

Fig. 8 Case 3: Comparison of predictions of the reduced-order model, the full model, and the CFD results from [62]. Variations with $t^* = tU/c$ of: (a) *LESP*, (b) lift coefficient, (c) drag coefficient (d) pitching-moment coefficient about one-third chord, (e) bound circulation, and (f) Fourier coefficient A_1.

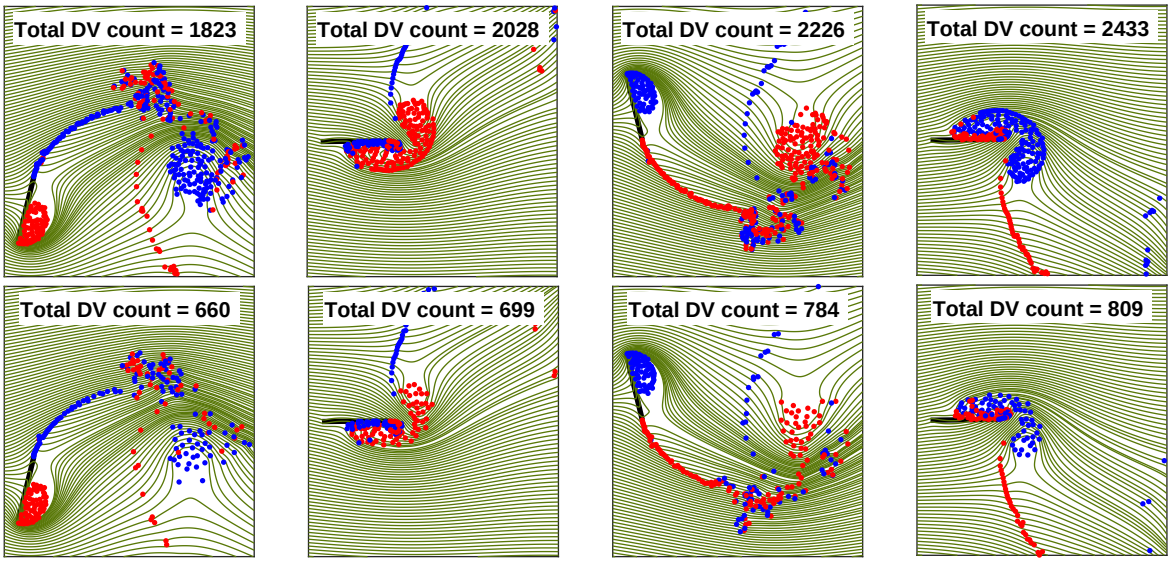

Fig. 9 Case 3: Comparison of flowfield results from full model (top) and the reduced-order model (bottom) at four time instants. Clockwise vortices are shown in blue and counterclockwise in red.

This case study demonstrates that the initiation and termination of the LEV structures as well as the alternating pattern of LEV shedding are accurately captured by the reduced-order model. Additionally, the convection of the LEV structures and their interactions with the airfoil and the TEV structures, as well as the vortex-structure interactions in the wake are replicated correctly as well. This is evident from the streamline patterns predicted by the reduced-order model, which are in good agreement with those predicted by the full model. The forces predicted by the two discrete-vortex methods agree excellently with each other and are in good agreement with the CFD results. It is to be highlighted that, compared to the full LDVM, the reduced-order model achieves results of comparable accuracy in a much smaller runtime of 120.2 seconds compared to a runtime of 490.7 seconds of the full model owing to a decrease in the discrete-vortex count from 2433 for the full model to 809 for the reduced-order model.

Summary of comparison of the two models

The evolution of execution time of the two models for the three cases is presented in Fig. 10. As the simulation advances, the discrete-vortex count in the flowfield of the full model increases linearly and the runtime per time step increases exponentially. On the other hand, the vortex count and the runtime per time step for the reduced-order model increases at a significantly slower rate. The difference between runtimes of the two models becomes significant for cases with larger number of discrete time steps, for instance case 3.

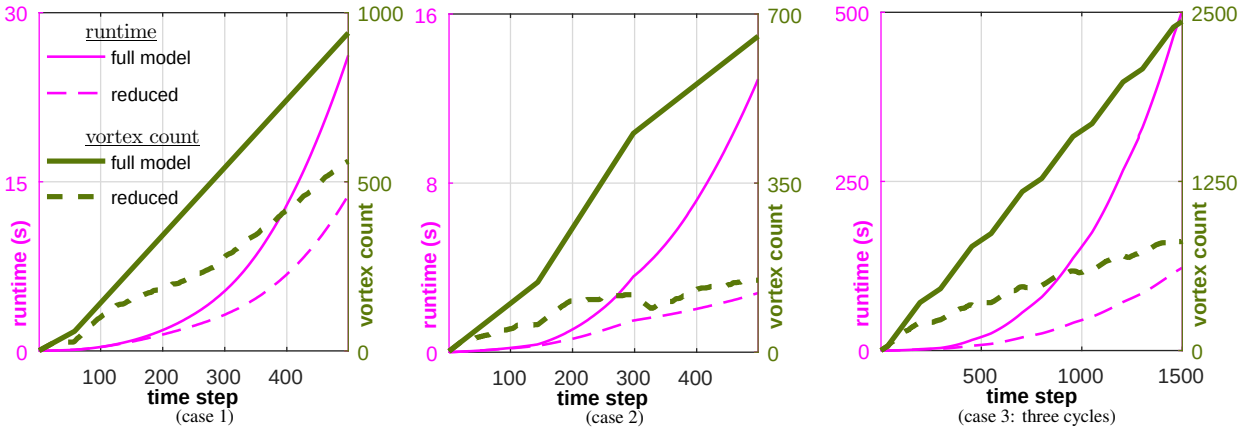

Fig. 10 Evolution of runtime and discrete-vortex count of the two models for the three cases.

Table 1 summarizes the discrete-vortex count in the final time step along with the percentage reductions in vortex count and runtime for each case. The runtimes reported have been averaged over several executions. It can be easily observed that the reduction in runtime is related to the reduction in discrete vortex count. For all cases, the time savings is slightly higher than the reduction in vortex count. Case 3 with a significant reduction in the discrete vortex count gives a higher reduction in runtime. It is clear that the reduction in vortex count is relatively small in case 1 and correspondingly the savings in runtime is smaller. At any time step, factors like separation between vortex pairs, the distance of the pairs from the airfoil, and their relative strengths collectively determine the vortices selected for amalgamation. Amalgamations are not guaranteed at every time step. This impacts the efficiency of model reduction because the computational cost involved in performing the search adversely affects the time saving.

More interestingly, Table 1 brings out the increasing effectiveness of model reduction with increasing number of cycles for the sinusoidal motion in case 3. To demonstrate this, a comparison of the discrete-vortex count and runtime of the two models is given in Table 1 for different number of cycles for the sinusoidal motion in case 3. It can be noticed that the runtime increases significantly for each additional cycle simulated. The savings in runtime obtained through model reduction become significant in such situations. Thus, the model reduction strategy presented in this paper will be highly advantageous for simulating motion kinematics for longer durations, especially for cases with significant vorticity shedding.

Case no.		vortex count		average runtime (s)		percentage reduction	
		LDVM	Reduced order	LDVM	Reduced order	vortex count	runtime
3	1	940	561	25.8	13.4	40.3	48.1
	2	655	149	12.6	2.7	77.3	78.6
	1 cycle	817	339	19.4	7.8	58.5	59.8
	2 cycles	1628	623	150.3	45.1	61.7	69.9
	3 cycles	2433	809	490.7	120.2	66.8	75.5

Table 1 Comparison of performance of the two models for the three cases.

V. Conclusions

In this paper, a model reduction strategy to improve the runtime of discrete-vortex methods was presented. Specifically, discrete-vortex pairs were amalgamated to reduce the number of vortices in the flowfield, thereby reducing the computational cost. Suitable vortex pairs were identified for amalgamation at each time step using a modified version of Spalart's criterion. Amalgamation was performed by placing the resultant vortex at an optimal location to ensure that the airfoil bound circulation and the leading-edge suction were not affected. This model reduction strategy was implemented in the discrete-vortex method called LDVM that was developed in earlier research for low-Reynolds-number airfoil flows dominated by LEV shedding.

Performance of the reduced-order model was compared against that of the full model for three case studies. The results from the reduced-order model were seen to be in good agreement with those of the full model, but with significantly smaller computation time compared to the latter. The case studies were chosen to demonstrate the capability of the reduced-order model to capture different flow features like intermittent LEV shedding, shear layer rollup, LEV pinch-off and vortex interactions. Streamline plots and discrete-vortex distributions at different time instants of motion showed that the reduced-order model was able to replicate the flowfield accurately using reduced number of discrete vortices. It was observed that the reduction in runtime was significant for cases with large number of discrete time steps and more number of discrete vortices in the flowfield. Thus, this model reduction strategy is highly suitable for simulating long-time kinematics that result in significant vorticity shedding. Aeroelastic interactions are potential problems where the reduced-order model can be expected to achieve significant reduction in runtime.

Finally, even though the model-reduction strategy is developed for the LDVM framework, the criteria for identification and amalgamation of vortex pairs are in terms of common kinematic and aerodynamic quantities. This formulation

provides for the easy modification of the current strategy for application to other discrete-vortex methods.

Funding Sources

The authors gratefully acknowledge the support of the U.S. Air Force Office of Scientific Research through grant FA 9550-17-1-0301 and the program manager Dr. Douglas Smith.

Acknowledgements

The authors thank Dr. Brenden Epps for the discussions that resulted in a refinement of the expressions for the force and moment coefficients in LDVM.

References

[1] von Kármán, T., and Sears, W., "Airfoil Theory for Non-Uniform Motion," *Journal of the Aeronautical Sciences*, Vol. 5, No. 10, 1938, pp. 379–390. doi:10.2514/8.674.

[2] Ellington, C. P., van den Berg, C., Willmott, A. P., and Thomas, A. L. R., "Leading-edge vortices in insect flight," *Nature*, Vol. 384, No. 1, 1996, pp. 626–630. doi:10.1038/384626a0.

[3] McCroskey, W. J., "Unsteady Airfoils," *Annual Review of Fluid Mechanics*, 1982, pp. 285–311. doi:10.1146/annurev.fl.14.010182.001441.

[4] Shyy, W., Aono, H., Chimakurthi, S. K., Trizila, P., Kang, C.-K., Cesnik, C. E. S., and Liu, H., "Recent progress in flapping wing aerodynamics and aeroelasticity," *Progress in Aerospace Sciences*, Vol. 46, No. 7, 2010, pp. 284–327. doi:10.1016/j.paerosci.2010.01.001.

[5] Ellington, C. P., "The novel aerodynamics of insect flight: applications to micro-air vehicles," *Journal of Experimental Biology*, Vol. 202, No. 23, 1999, pp. 3439–3448.

[6] Dickinson, M. H., and Gotz, K. G., "Unsteady aerodynamic performance of model wings at low Reynolds numbers," *Journal of Experimental Biology*, Vol. 174, No. 1, 1993, pp. 45–64.

[7] Taha, H. E., Hajj, M. R., and Nayfeh, A. H., "Flight dynamics and control of flapping-wing MAVs: a review," *Nonlinear Dynamics*, Vol. 70, No. 2, 2012, pp. 907–939. doi:10.1007/s11071-012-0529-5.

[8] Platzer, M., and Jones, K., "Flapping Wing Aerodynamics – Progress and Challenges," AIAA Paper 2006–500, 2006. doi:10.2514/6.2006-500.

[9] Bryant, M., and Garcia, E., "Modeling and testing of a novel aeroelastic flutter energy harvester," *Journal of Vibration and Acoustics*, Vol. 133, No. 1, 2011. doi:10.1115/1.4002788.

[10] Young, J., Ashraf, M. A., Lai, J. C. S., and Platzer, M. F., "Numerical Simulation of Fully Passive Flapping Foil Power Generation," *AIAA Journal*, Vol. 51, No. 11, 2013, pp. 2727–2739. doi:10.2514/1.J052542.

[11] Dunnmon, J. A., Stanton, S. C., Mann, B. P., and Dowell, E. H., "Power extraction from aeroelastic limit cycle oscillations," *Journal of Fluids and Structures*, Vol. 27, No. 8, 2011, pp. 1182–1198. doi:10.1016/j.jfluidstructs.2011.02.003.

[12] Kinsey, T., Dumas, G., Lalande, G., Ruel, J., Mehut, A., Viarouge, P., Lemay, J., and Jean, Y., "Prototype testing of a hydrokinetic turbine based on oscillating hydrofoils," *Renewable Energy*, Vol. 36, No. 6, 2011, pp. 1710–1718. doi:10.1016/j.renene.2010.11.037.

[13] Wagner, H., "Über die Entstehung des dynamischen Auftriebes von Tragflügeln," *ZaMM*, Vol. 5, No. 1, 1925, pp. 17–35.

[14] Theodorsen, T., "General Theory of Aerodynamic Instability and the Mechanism of Flutter," NACA Rept. 496, 1935.

[15] McGowan, G. Z., Granlund, K., Ol, M. V., Gopalarathnam, A., and Edwards, J. R., "Investigations of lift-based pitch-plunge equivalence for airfoils at low Reynolds numbers," *AIAA Journal*, Vol. 49, No. 7, 2011, pp. 1511–1524. doi:10.2514/1.J050924.

[16] Ol, M. V., Bernal, L., Kang, C. K., and Shyy, W., "Shallow and deep dynamic stall for flapping low Reynolds number airfoils," *Experiments in fluids*, Vol. 46, No. 5, 2009, pp. 883–901. doi:10.1007/s00348-009-0660-3.

[17] Garmann, D. J., and Visbal, M. R., "Numerical investigation of transitional flow over a rapidly pitching plate," *Physics of Fluids*, Vol. 23, 2011, p. 094106. doi:10.1063/1.3626407.

[18] Granlund, K., Ol, M. V., and Bernal, L. P., "Unsteady pitching flat plates," *Journal of Fluid Mechanics*, Vol. 733, 2013, p. R5. doi:10.1017/jfm.2013.444.

[19] Pitt Ford, C. W., and Babinsky, H., "Lift and the leading-edge vortex," *Journal of Fluid Mechanics*, Vol. 720, 2013, pp. 280–313. doi:10.1017/jfm.2013.28.

[20] Baik, Y. S., Bernal, L. P., Granlund, K., and Ol, M. V., "Unsteady force generation and vortex dynamics of pitching and plunging aerofoils," *Journal of Fluid Mechanics*, Vol. 709, 2012, pp. 37–68. doi:10.1017/jfm.2012.318.

[21] Rival, D. E., Kriegseis, J., Schaub, P., Widmann, A., and Tropea, C., "A criterion for vortex separation on unsteady aerodynamic profiles," AIAA Paper 2013-0836, January 2013. doi:10.2514/6.2013-836.

[22] Visbal, M. R., and Shang, J. S., "Investigation of the flow structure around a rapidly pitching airfoil," *AIAA Journal*, Vol. 27, No. 8, 1989, pp. 1044–1051. doi:10.2514/3.10219.

[23] Ghosh Choudhuri, P., Knight, D., and Visbal, M. R., "Two-dimensional unsteady leading-edge separation on a pitching airfoil," *AIAA Journal*, Vol. 32, No. 4, 1994, pp. 673–681. doi:10.2514/3.12040.

[24] Katz, J., "Discrete vortex method for the non-steady separated flow over an airfoil," *Journal of Fluid Mechanics*, Vol. 102, No. 1, 1981, pp. 315–328. doi:10.1017/S0022112081002668.

[25] Ramesh, K., Gopalarathnam, A., Granlund, K., Ol, M. V., and Edwards, J. R., "Discrete-vortex method with novel shedding criterion for unsteady airfoil flows with intermittent leading-edge vortex shedding," *Journal of Fluid Mechanics*, Vol. 751, 2014, pp. 500–538. doi:10.1017/jfm.2014.297.

[26] Wang, C., and Eldredge, J. D., "Low-order phenomenological modeling of leading-edge vortex formation," *Theoretical Computational Fluid Dynamics*, Vol. 27, 2013, pp. 577–598. doi:10.1007/s00162-012-0279-5.

[27] Clements, R. R., and Maull, D. J., "The representation of sheets of vorticity by discrete vortices," *Progress in Aerospace Sciences*, Vol. 16, No. 2, 1975, pp. 129–146. doi:10.1016/0376-0421(75)90013-5.

[28] Saffman, P. G., and Baker, G. R., "Vortex interactions," *Annual Review of Fluid Mechanics*, Vol. 11, No. 1, 1979, pp. 95–121. doi:10.1146/annurev.fl.11.010179.000523.

[29] Sarpkaya, T., "An inviscid model of two-dimensional vortex shedding for transient and asymptotically separated flow over an inclined plate," *Journal of Fluid Mechanics*, Vol. 68, No. 1, 1975, pp. 109–128. doi:10.1017/S0022112075000717.

[30] Clements, R. R., "An inviscid model of two-dimensional vortex shedding," *Journal of Fluid Mechanics*, Vol. 57, No. 2, 1973, pp. 321–336. doi:10.1017/S0022112073001187.

[31] Kiya, M., and Arie, M., "A contribution to an inviscid vortex-shedding model for an inclined flat plate in uniform flow," *Journal of Fluid Mechanics*, Vol. 82, No. 2, 1977, pp. 223–240. doi:10.1017/S0022112077000627.

[32] Leonard, A., "Vortex methods for flow simulation," *Journal of Computational Physics*, Vol. 37, No. 3, 1980, pp. 289–335. doi:10.1016/0021-9991(80)90040-6.

[33] Ansari, S. A., Zbikowski, R., and Knowles, K., "Nonlineary unsteady aerodynamic model for insect-like flapping wings in hover. Part 1: Methodology and analysis," *Proceedings of the Institution of Mechanical Engineers, Part G: Journal of Aerospace Engineering*, Vol. 220, No. 3, 2006, pp. 61–83. doi:10.1243/09544100JAERO49.

[34] Hammer, P., Altman, A., and Eastep, F., "Validation of a Discrete Vortex Method for Low Reynolds Number Unsteady Flows," *AIAA Journal*, Vol. 52, No. 3, 2014, pp. 643–649. doi:10.2514/1.J052510.

[35] Brown, C. E., and Michael, W. H., "Effect of leading edge separation on the lift of a delta wing," *Journal of Aeronautical Sciences*, Vol. 21, 1954, pp. 690–694. doi:10.2514/8.3180.

[36] Milano, M., and Gharib, M., "Uncovering the physics of flapping plates with artificial evolution," *Journal of Fluid Mechanics*, Vol. 534, 2005, pp. 403–409. doi:10.1017/S0022112005004842.

[37] Rival, D., Prangemeier, T., and Tropea, C., "The influence of airfoil kinematics on the formation of leading-edge vortices in bio-inspired flight," *Experiments in Fluids*, Vol. 46, 2009, pp. 823–833. doi:10.1007/s00348-008-0586-1.

[38] Rival, D., Kriegseis, J., Schaub, P., Widmann, A., and Tropea, C., "Characteristic length scales for vortex detachment on plunging profiles with varying leading-edge geometry," *Experiments in Fluids*, Vol. 55, No. 1, 2014, p. 18. doi:10.1007/s00348-013-1660-x.

[39] Darakananda, D., Eldredge, J. D., Colonius, T., and Williams, D. R., "A vortex sheet/point vortex dynamical model for unsteady separated flows," AIAA Paper 2016–2072, January 2016. doi:10.2514/6.2016-2072.

[40] Antonini, E. G. A., Bedon, G., Betta, S. D., Michelini, L., Castelli, M. R., and Benini, E., "Innovative Discrete-Vortex Model for Dynamic Stall Simulations," *AIAA Journal*, Vol. 53, 2015, pp. 479–485. doi:10.2514/1.J053430.

[41] SureshBabu, A., Ramesh, K., and Gopalarathnam, A., "Model Reduction in Discrete Vortex Methods for 2D Unsteady Aerodynamic Flows," AIAA Paper 2016-4163, June 2016. doi:10.2514/6.2016-4163.

[42] Howe, M. S., "Emendation of the Brown Michael equation, with application to sound generation by vortex motion near a half-plane," *Journal of Fluid Mechanics*, Vol. 329, 1996, pp. 89–101. doi:10.1017/S002211209600883X.

[43] Cortelezzi, L., and Leonard, A., "Point vortex model of the unsteady separated flow past a semi-infinte plate with transverse motion," *Fluid Dynamics Research*, Vol. 11, 1993, pp. 263–295. doi:10.1016/0169-5983(93)90013-Z.

[44] Cortelezzi, L., "A theoretical and computational study on active wake control," Ph.D. thesis, California Institute of Technology, 1992.

[45] Moore, D. W., "A numerical study of the roll-up of a finite vortex sheet," *Journal of Fluid Mechanics*, Vol. 63, No. 2, 1974, pp. 225–235. doi:10.1017/S002211207400111X.

[46] Michelin, S., and Llewellyn Smith, S. G., "An unsteady point vortex method for coupled fluid–solid problems," *Theoretical and Computational Fluid Dynamics*, Vol. 23, No. 2, 2009, pp. 127–153. doi:10.1007/s00162-009-0096-7.

[47] Spalart, P. R., "Vortex Methods for separated flows," NASA technical memorandum 100068, 1988. N88-26342.

[48] Nair, A. G., and Taira, K., "Network-theoretic approach to sparsified discrete vortex dynamics," *Journal of Fluid Mechanics*, Vol. 768, 2015, pp. 549–571. doi:10.1017/jfm.2015.97.

[49] Xia, X., and Mohseni, K., "Modeling of 2D Unsteady Motion of a Flat Plate using Potential Flow," AIAA Paper 2013-2819, San Diego, June 2013. doi:10.2514/6.2013-2819.

[50] Ramesh, K., Murua, J., and Gopalarathnam, A., "Limit-cycle oscillations in unsteady flows dominated by intermittent leading-edge vortex shedding," *Journal of Fluids and Structures*, Vol. 55, No. Supplement C, 2015, pp. 84 – 105. doi:10.1016/j.jfluidstructs.2015.02.005.

[51] Katz, J., and Plotkin, A., *Low-Speed Aerodynamics*, Cambridge Aerospace Series, 2001. doi:10.1017/CBO9780511810329.

[52] Ramesh, K., Gopalarathnam, A., Edwards, J. R., Ol, M. V., and Granlund, K., "An unsteady airfoil theory applied to pitching motions validated against experiment and computation," *Theoretical and Computational Fluid Dynamics*, Vol. 27, No. 6, 2013, pp. 843–864. doi:10.1007/s00162-012-0292-8.

[53] Epps, B. P., and Roesler, B. T., "Vortex Sheet Strength in the Sears, Küssner, Theodorsen, and Wagner Aerodynamics Problems," *AIAA Journal*, Vol. 56, No. 3, 2018, pp. 889–904. doi:10.2514/1.J056399.

[54] Epps, B. P., and Greeley, D. S., "A Quasi-Continuous Vortex Lattice Method for Unsteady Aerodynamics Analysis," *AIAA Paper 2018-0815*, 2018. doi:10.2514/6.2018-0815.

[55] Xia, X., and Mohseni, K., "Unsteady aerodynamics and vortex-sheet formation of a two-dimensional airfoil," *Journal of Fluid Mechanics*, Vol. 830, 2017, p. 439–478. doi:10.1017/jfm.2017.513.

[56] Vatistas, G. H., Kozel, V., and Mih, W. C., "A simpler model for concentrated vortices," *Experiments in Fluids*, Vol. 11, No. 1, 1991, pp. 73–76. doi:10.1007/BF00198434.

[57] Aggarwal, S., "An Inviscid Numerical Method for Unsteady Flows Over Airfoils and Wings to Predict the Onset of Leading Edge Vortex Formation," Master's thesis, North Carolina State University, Raleigh, NC, November 2013.

[58] Eldredge, J. D., "Numerical simulation of the fluid dynamics of 2D rigid body motion with the vortex particle method," *Journal of Computational Physics*, Vol. 221, No. 2, 2007, pp. 626–648. doi:10.1016/j.jcp.2006.06.038.

[59] Eldredge, J. D., Wang, C., and Ol, M. V., "A Computational Study of a Canonical Pitch-up, Pitch-down Wing Maneuver." AIAA paper 2009-3687, 2009. doi:10.2514/6.2009-3687.

[60] Ramesh, K., Granlund, K., Ol, M. V., Gopalarathnam, A., and Edwards, J. R., "Leading-edge flow criticality as a governing factor in leading-edge vortex initiation in unsteady airfoil flows," *Theoretical and Computational Fluid Dynamics*, Vol. 32, No. 2, 2018, pp. 109–136. doi:10.1007/s00162-017-0442-0.

[61] Smits, A. J., and Lim, T. T. (eds.), *Flow Visualization: Techniques and Examples*, Imperial College Press, 2000. doi:10.1142/p167.

[62] Kinsey, T., and Dumas, G., "Parametric study of an oscillating airfoil in a power-extraction regime," *AIAA Journal*, Vol. 46, No. 6, 2008, pp. 1318–1330. doi:10.2514/1.26253.